A New Configuration of Polarization-Rotating Dual-Beam Interferometer for Space Use

Takeshi Manabe, *Member, IEEE*, Junji Inatani, Axel Murk, Richard J. Wylde, Masumichi Seta, and Derek H. Martin

***Abstract*—This paper presents a new configuration of quasi-optical polarization-rotating dual-beam interferometer, which uses a pair of frequency-selective polarizers (FSPs) consisting of a wire-grid placed in front of a flat mirror, and has a function similar to the conventional Martin–Puplett interferometer (MPI). Advantages of this new configuration over the conventional MPI are lower residual reflection at the input and output ports and suitability to fixed-tuned applications. An experiment has shown it to have an MPI-like frequency characteristic as calculated. Careful machining was successful in achieving accuracy needed for a specified filter characteristic. This FSP-based quasi-optical device is to be used as a sideband separator in a space-borne submillimeter receiver for atmospheric research.**

***Index Terms*—Martin–Puplett interferometers (MPIs), polarization-rotating dual-beam interferometers, quasi-optical filters, sideband separators.**

I. Introduction

In the millimeter- and submillimeter-wave regions above 100 GHz, quasi-optical frequency selective devices, such as the Martin–Puplett interferometer (MPI) and its variants, are widely used for filtering and diplexing at the front end of receivers for radio astronomy and atmospheric remote sensing [1]–[5]. The MPI [6], [7] is a polarization-rotating dual-beam interferometer consisting of a wire grid and two dihedral corner reflectors. The MPI has a low insertion loss and its frequency characteristics can be easily tuned by changing the optical path difference between the two interferometer arms.

There are, however, two aspects of the standard MPI that can lead to problems when used in a fixed-tuned receiver for a space-borne sensor. Firstly, the two optical paths through the interferometer are spatially separated over distances that greatly exceed the final path difference. If the path difference is to be determined to an accuracy better than a few hundredths of the wavelength, i.e., on the order of 1 μm or less at submillimeter wavelengths, the dimensions of the whole interferometer must be machined to extremely high precision, and must remain stable over the whole temperature range of operation. This would be very difficult to achieve without an active tuning mechanism. Secondly, nonideal performance of the wire grids in transmission and reflection, which must be expected at high submillimeter-wave frequencies, gives rise to residual reflections from the input and output ports; this leads to standing waves in the receiver optics and a consequent reduction in receiver sensitivity.

In this paper, we introduce a new configuration for a quasi-optical polarization-rotating dual-beam interferometer, which is free from these deficiencies of the MPI configuration. The new configuration consists of two frequency-selective polarizers (FSPs) in tandem. An FSP comprises a planer wire grid backed by a parallel plane reflecting mirror maintained at a precisely determined separation measuring a few wavelengths, and is used in reflection.

This paper is organized as follows. The configuration and operational principle of this newly proposed FSP-based interferometer are introduced in Section II, and some advantages over the standard MPI are presented. The transmission characteristics for incident plane waves are derived in Section III and the significance of multiple reflection within each FSP attributable to nonideal performance of the wire grids is demonstrated in Section IV. The effects of diffraction due to finite beamwidth on the transmission characteristics are discussed in Section V. In Section VI, the results of the theoretical model calculations are compared with the results of measurements made on a prototype model of a sideband separator that incorporate the new configuration and operates at submillimeter-wave frequencies around 640 GHz. Finally, our conclusions are presented in Section VII.

II. Configuration and Principle

The configuration of the newly proposed FSP-based dual-beam interferometer is shown in Fig. 1 and compared there with the standard MPI configuration. We first describe the operation of the interferometer assuming that each wire grid performs ideally, i.e., totally reflects one linear-polarization component of an incident collimated beam (that with E-field parallel to the wires), and totally transmits the orthogonally polarized component.

The interferometer has two FSPs in tandem. A collimated incident beam, on transmission through the wire grid at the input port, is linearly polarized in the plane, making an angle of 45° with respect to the normal to the page. The wires in the grid of the first frequency-selective polarizer (FSP1) are normal to the page, and the beam is, therefore, divided into two beams of

Manuscript received August 10, 2002; revised October 8, 2002. The work of A. Murk was supported in part by the Swiss National Science Foundation under Grant 2000–063897.00.

T. Manabe and M. Seta are with the Communications Research Laboratory, Tokyo 184-8795, Japan (e-mail: manabe@crl.go.jp; seta@crl.go.jp).

J. Inatani is with the National Space Development Agency of Japan, Ibaraki 305-8505, Japan (e-mail: inatani.junji@nasda.go.jp).

A. Murk is with the Institute of Applied Physics, University of Berne, CH-3012 Berne, Switzerland (e-mail: axel.murk@mw.iap.unibe.ch).

R. J. Wylde is with Thomas Keating Ltd., West Sussex RH14 9SH, U.K. and also with the Department of Physics and Astronomy, University of St. Andrews, Fife KY16 9SS, U.K. (e-mail: R.Wylde@terahertz.co.uk).

D. H. Martin is with the Department of Physics, Queen Mary and Westfield College, London E1 4NS, U.K. (d.h.martin@qmul.ac.uk).

Digital Object Identifier 10.1109/TMTT.2003.812567

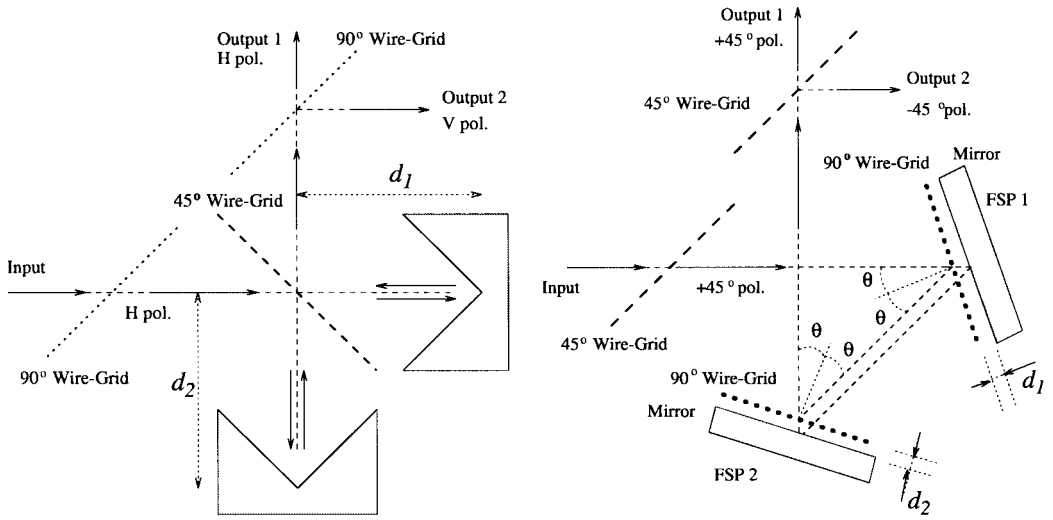

Fig. 1. (a) Standard MPI configuration. (b) Newly proposed FSP-based configuration.

equal amplitude: a reflected s-polarized beam (electric field E_s perpendicular to the page) and a transmitted p-polarized beam (electric field E_p parallel to the page). The transmitted p-polarized beam is then reflected at the plane reflector behind the wire grid, passes through the wire grid again, to be propagated with the s-polarized beam superposed, but laterally displaced, toward the second frequency-selective polarizer (FSP2).

The wires of the grid of FSP2 are normal to the page so the s-component is again reflected at the grid. The p-component is again transmitted at the grid, reflected at the plane reflector, and transmitted through the grid. The emergent s- and p-polarized beams are now superposed again, but with little lateral displacement from each other if the spacings in the two FSPs are not equal.

The FSP1 has thus served as beam divider and the FSP2 as beam combiner. The s- and p-polarized beams have travelled different distances, however, so the recombined beam is elliptically polarized, the ellipticity and the orientation of the major axis being determined by the phase difference of the two beams.

The recombined beam is analyzed by the wire grid at the output port. The wires of the grid are at 45° to the normal to the page; a transmitted beam polarized at 45° to the normal is directed to output port 1 and a reflected beam polarized at $-45°$ to the normal is directed to output port 2.

When the phase difference Φ between the s and p components of the recombined beam is an even integer multiple of π, the beams interfere constructively in output port 1 and destructively in output port 2. When the phase difference Φ is an odd integer multiple of π, the beams interfere destructively in output port 1 and constructively in output port 2. The transmission characteristics of this FSP-based configuration are thus exactly the same as those of the standard MPI configuration [7] when ideal performance of wire grids is assumed (there is an significant difference in characteristics when the nonideality of the grids is taken into account, as will be discussed in the following sections).

Though the layouts of the two configurations shown in Fig. 1 may have a superficial resemblance to each other, the spatial disposition of the two beam paths is, in fact, very different in the two configurations. In the FSP-based configuration, the two beams follow essentially the same path, except within the FSPs where the path difference is established. For that reason, though the dimensions *within* each FSP must be stable to submicrometer precision, it is not essential that the separation *between* the two FSPs be stable to the same absolute precision. Careful design and fabrication of the FSPs should ensure this; only the structure of the FSP needs to be made of a low thermal expansion material such as Invar, and the rest of the structure supporting the two FSPs could be made of less thermally stable materials. In the MPI configuration, on the other hand, the two beams follow spatially well-separated paths from wire grid to dihedral reflector and back, each path being several tens of millimeters in length. With an MPI, it would be necessary to maintain these overall dimensions to submicrometer precision. In the adverse kinetic and thermal environment of a space-borne receiver, the first major advantage of the FSP-based interferometer over an MPI configuration—the saving in mass for a space-borne receiver would be highly significant.

Thus far, we have assumed the performance of wire grids to be ideal. Real wire grids will not be ideal linear polarizers, at each there will be some leakage of cross-polarized signal power in reflection and in transmission. In the standard MPI configuration, such leakage results in some return of signal power to the source. Though such return might be at a low level, it can result in standing waves within the receiver optics with a serious degradation of receiver performance. In the proposed FSP-based interferometer, on the other hand, such leakage does not result in the return of any power to the source — it is clear that all signal power is transported forward. This is the second major advantage of the proposed FSP-based interferometer. The nonideality of the grids does have another consequence — there will be some multiple reflection of signal power between the wire grid and the mirror within each FSP —but, as will be seen in Section IV, that can itself be used to an advantage provided it is well understood.

III. Transmission Characteristics of FSP-Based Interferometer for Plane Waves

First, here, let us consider an idealized case when a plane wave is incident on the proposed interferometer consisting of two FSPs with infinite extent. Throughout this paper, we assume the direction of the grid wires of the FSPs to be perpendicular to the plane of incidence, as shown in Fig. 1(b).

The essential characteristics of our device are the complex amplitude transmission functions T_1 and T_2 for plane-wave propagation from the input polarizer to output ports 1 and 2, respectively.

Since the wire grids of the FSPs are oriented perpendicular to the plane of incidence, it is convenient in the theoretical analysis to decompose the input polarization into s- and p-polarized basis because the reflection by each FSP can be expressed by complex amplitude reflection coefficients R_s and R_p for respective components without cross-polar coupling.

If the wire grid had no cross-polar leakage, the proposed FSP-based interferometer would be a dual-beam interferometer. The leakage components give rise to some multiple reflections within each FSP, however, and this has an appreciable effects on the FSP's plane-wave transmission characteristics, as shown in Section IV.

By using these reflection coefficients, R_s and R_p for the two FSPs given in Appendix A, the complex amplitude transmission functions for plane-wave incidence are expressed for two orthogonally polarized output ports as

$$T_1 = \frac{R_{s1}R_{s2} + R_{p1}R_{p2}}{2} \text{ for output port 1} \tag{1}$$

and

$$T_2 = \frac{R_{s1}R_{s2} - R_{p1}R_{p2}}{2} \text{ for output port 2} \tag{2}$$

where subscripts 1 and 2 attached to the reflection coefficients R_s and R_p refer to FSP1 and FSP2, respectively.

IV. Numerical Example of a Design of FSP-Based Interferometer for Sideband Separator

Here, as an example of design of an FSP-based interferometer, we introduce a numerical design of a sideband separator, which was made for a submillimeter-wave superconductor–insulator–superconductor (SIS) receiver of the Superconducting Submillimeter-Wave Limb-Emission Sounder (SMILES) to be aboard the Japanese Experiment Module (JEM) of the International Space Station [8], [9].

From scientific requirements to observe as many molecular species relating to stratospheric ozone depletion as possible within a limited bandwidth of the onboard spectrometer, JEM/SMILES is designed to achieve single-sideband observation in two submillimeter-wave bands, i.e., 624.32–626.32 and 649.12–650.32 GHz, simultaneously as lower sideband (LSB) and upper sideband (USB), respectively, by two SIS mixers with a local-oscillator set at 637.32 GHz. The function of the sideband separator is to demultiplex the input submillimeter-wave signals into the two sidebands, that in the LSB being delivered to one output port, and that in the USB to the other output port, as shown in Fig. 1(b), for simultaneous heterodyne detection by two SIS mixers. For this simultaneous heterodyne detection, the SMILES sideband separator is also designed to function as a diplexer for the local-oscillator signal, at the frequency around the crossover frequency of T_1 and T_2 that is injected through the input 45° wire grid and is coupled to both SIS mixers with local power split as evenly as possible.

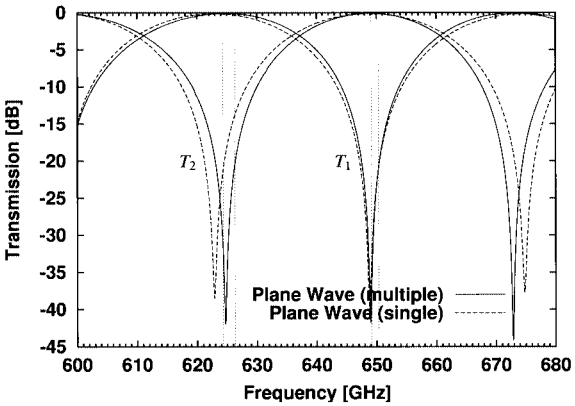

Fig. 2. Transmission characteristics T_1 and T_2 of the FSP-based interferometer ($d_1 = 1.543$ mm, $d_2 = 1.573$ mm, $\sigma_g^{-1} = 5.5 \times 10^{-8}\ \Omega \cdot$ m, $\sigma_m^{-1} = 7.9 \times 10^{-7}\ \Omega \cdot$ m) for plane-wave incidence. Solid curves show the case when multiple reflections between wire grid and reflecting mirror are taken into account, while dotted curves show the case when multiple reflections are ignored.

In the calculation of the transmission characteristics of the sideband separator, the diameter and pitch of the wire are assumed to be 10 and 25 μm, respectively, and the angle of incidence to the FSP is assumed to be 22.5°. The plane of incidence is assumed to be parallel to the plane spanned by the surface normals of the wire grids of two FSPs. The plane of polarization of incident wave is assumed to make an angle of 45° with respect to the plane of incidence. The wire grid and mirror are assumed to be made of tungsten and Invar whose resistivities are $5.5 \cdot 10^{-8}\ \Omega \cdot$ m and $7.9 \cdot 10^{-7}\ \Omega \cdot$ m, respectively [10].

After a not-exhaustive search for combinations of the spacings (d_1 and d_2) of two FSPs, it was found that the combination of $d_1 = 1.543$ mm and $d_2 = 1.573$ mm is a reasonable choice by which we can achieve image rejection better than 15 dB within LSB and USB of the SMILES observation bands and also set the difference in local coupling coefficient at 637.32 GHz to be less than 0.5 dB, simultaneously. The solid curves in Fig. 2 show the transmission characteristics T_1 and T_2 calculated for this combination. In Fig. 2, corresponding transmission characteristics calculated considering only the two dominant interferometric paths by ignoring multiple reflections between the wire grid and mirror are also shown by the dotted curves for comparison. Fig. 2 indicates that the multiple reflections between the wire grid and mirror within each FSP has a significant effects on the transmission characteristics of the FSP-based interferometer and should, therefore, be taken into account in its design.

In the standard MPI, which has only one degree of freedom for frequency tuning, the transmission and rejection peak frequencies of T_1 and T_2 should be integer multiples of the minimum separation of these frequencies. In this case, we, therefore, are unable to set adjacent transmission and rejection peaks at arbitrary frequencies. This also corresponds to the case when

the multiple reflection is ignored in our interferometer, as is shown by dotted curves in Fig. 2. On the other hand, in our interferometer, it can be said that we can gain a little more degree of freedom in tuning transmission and rejection frequencies by virtue of the effects of multiple reflection within each FSPs combined with the two degrees of freedom (d_1 and d_2).

V. Diffraction Effects

Thus far, we have ignored the effects of diffraction. Here, we consider the effects of diffraction by assuming that the incident wave is a fundamental-mode Gaussian beam of waist radius w_0 and that the sizes of the FSPs are large enough not to truncate the beam. In considering the effects of diffraction, we have to take account of the imperfect beam overlap, as a combined result of axial beam shift due to different traveling distance and lateral walkoff of each multiply reflected beam component separately, when they interfere to form the output beam after being reflected by two FSPs.

By considering each multipath component with its axial beam shift and walkoff for the combination of two FSPs comprising the FSP-based interferometer, the complex amplitude transmission functions of the FSP-based interferometer for s- and p-polarized waves can be obtained by inserting the respective coefficients r, t, and r_m for s- and p-polarized waves given by (16), (17), (14), and (15), respectively, in Appendix A into

$$\begin{aligned} T =& \xi_{00}\zeta_{00}r^2 + t^2\sum_{p=1}^{\infty}\xi_{p0}\zeta_{p0}(r_m r)^p \\ &+ t^2\sum_{q=1}^{\infty}\xi_{0q}\zeta_{0q}(r_m r)^q \\ &+ t^4\sum_{p=1}^{\infty}\sum_{q=1}^{\infty}\xi_{pq}\zeta_{pq}(r_m r)^{p+q-2}r^2. \end{aligned} \tag{3}$$

The first term of (3) represents the path reflected at the wire grids at both FSP1 and FSP2 without experiencing reflections by mirrors of FSPs. The second and third terms represent the paths that experience single and multiple reflections within either FSP1 or FSP2. The last term represents the paths that experience single and multiple reflections within both FSPs. In (3), ξ_{pq} and ζ_{pq} represent the effects of axial beam offset and lateral walkoff of each path [11], respectively, given by[1]

$$\xi_{pq} = \frac{\exp\left(\dfrac{i2\pi\Delta_{\rm ax}}{\lambda}\right)}{1 + i\dfrac{\lambda\Delta_{\rm ax}}{2\pi w_0^2}} \tag{4}$$

and

$$\zeta_{pq} = \exp\left(-\frac{1}{2}\frac{\left(\dfrac{\Delta_l}{w_0}\right)^2}{1 + i\dfrac{\lambda\Delta_{\rm ax}}{2\pi w_0^2}}\right) \tag{5}$$

[1]The time dependence of electromagnetic field is assumed to be $\exp(-i\omega t)$ and is omitted throughout this paper.

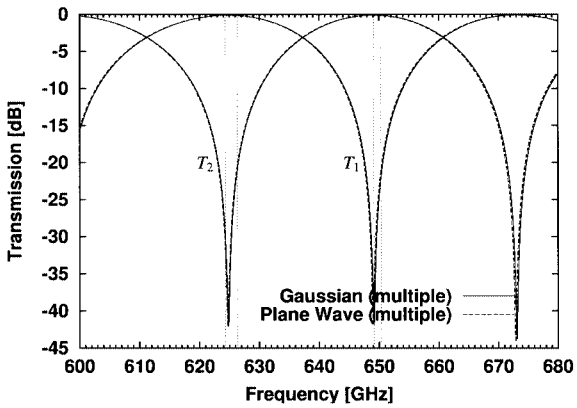

Fig. 3. Transmission characteristics T_1 and T_2 of the FSP-based interferometer ($d_1 = 1.543$ mm, $d_2 = 1.573$ mm, $\sigma_g^{-1} = 5.5 \times 10^{-8}\ \Omega \cdot$ m, $\sigma_m^{-1} = 7.9 \times 10^{-7}\ \Omega \cdot$ m) for a fundamental-mode Gaussian beam with a beamwidth of $w_0 = 4.61$ mm (solid curves) are compared with those for plane-wave incidence (dotted curves).

where $\Delta_{\rm ax}$ and Δ_l are the axial beam offset and lateral walkoff, respectively, given by

$$\Delta_{\rm ax} = 2(pd_1 + qd_2)\cos\theta \tag{6}$$

and

$$\Delta_l = 2(pd_1 - qd_2)\sin\theta. \tag{7}$$

The transmission characteristics of the FSP-based interferometer consisting of two FSPs with different grid-mirror spacings are calculated for two orthogonal polarizations by the following equations:

$$T_1 = \frac{T_p + T_s}{2} \text{ for output port 1} \tag{8}$$

and

$$T_2 = \frac{T_p - T_s}{2} \text{ for output port 2} \tag{9}$$

where T_s and T_p are the transmission coefficients given by (3) for s- and p-polarized wave incidence, respectively.

The transmission characteristics T_1 and T_2 calculated for an incident Gaussian beam whose beam waist radius w_0 is 4.61 mm are shown in Fig. 3 by solid curves. In Fig. 3, the corresponding transmission characteristics for the case of plane-wave incidence (solid curves in Fig. 2) are also shown again by dotted curves for comparison. To make the comparison clearer, the transmission characteristics around the center of the transmission bands are magnified in Figs. 4 and 5. It is found in Figs. 4 and 5 that the effect of diffraction is not negligible giving rise to a frequency shift of approximately 150 MHz on the transmission characteristics. Therefore, the effect of diffraction should only be taken into account by using (3), (8), and (9) in detailed design of FSP-based interferometers.

VI. Comparison With Measurements

A prototype model of a sideband separator based on the FSP-based interferometer has been fabricated for the JEM/SMILES

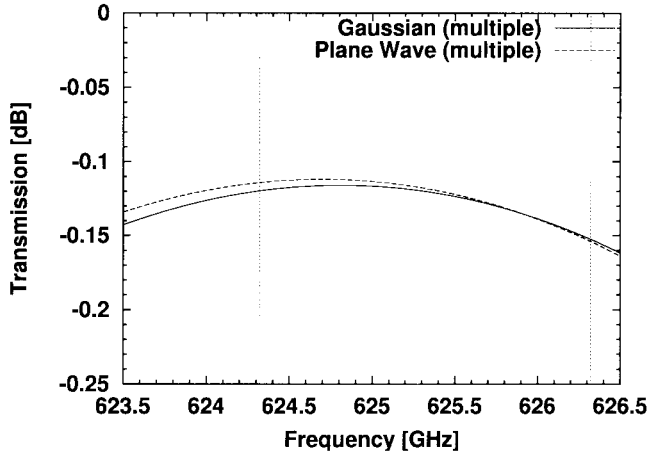

(a)

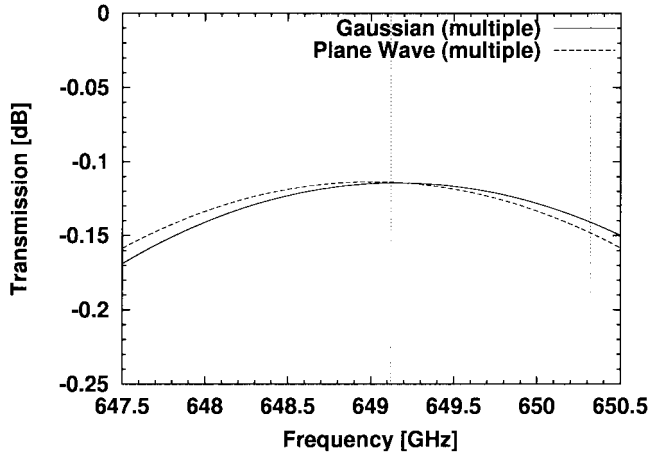

(b)

Fig. 4. Enlarged views of Fig. 3 for the bandpass characteristics around the: (a) LSB and (b) USB of the FSP-based sideband separator with $d_1 = 1.543$ mm and $d_2 = 1.573$ mm.

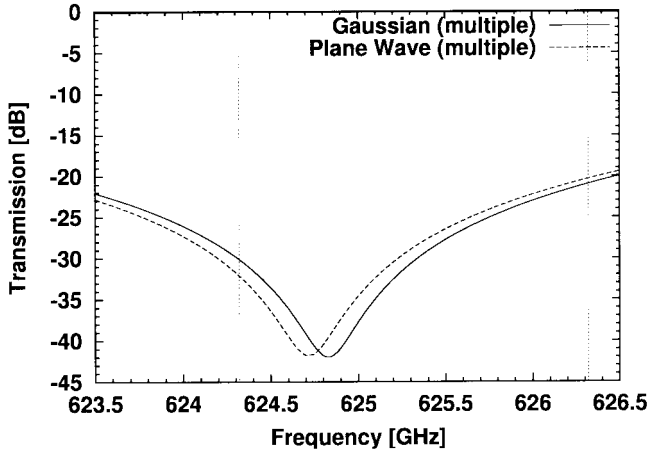

(a)

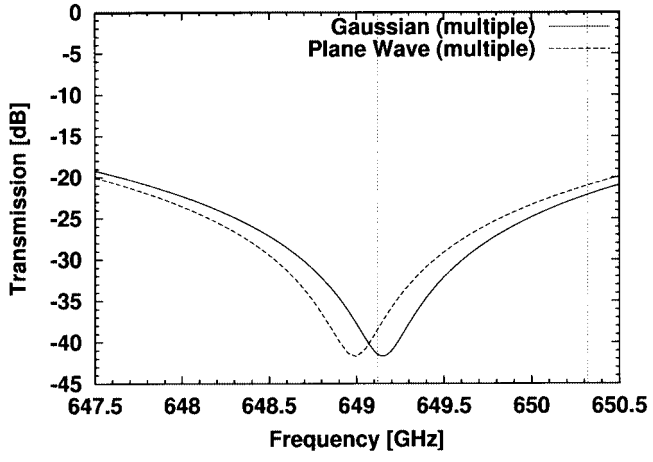

(b)

Fig. 5. Enlarged views of Fig. 3 for the band rejection characteristics around the: (a) LSB and (b) USB of the FSP-based sideband separator with $d_1 = 1.543$ mm and $d_2 = 1.573$ mm.

submillimeter-wave receiver to experimentally verify the theoretical model calculations.

Each FSP was made up of a frame structure composed of a grid frame and a backing reflector plate on which a grid with tungsten wire of 10-μm diameter was wound with a pitch of 25 μm. Both the grid frame and backing reflector plate were made of Invar to keep the grid-mirror spacing thermally stable. Before winding the grid, the surfaces of the grid frame and reflector were ground and lapped flat, and were made parallel to achieve a tolerance of better than 2 μm for the intended spacing d between the plane of the wire grid and reflector. These two FSPs were held by an aluminum frame structure so as to face with an angle of 45° to each other in order to make the angle of incidence θ in Fig. 1 to be 22.5°. The grid-mirror spacings d_1 and d_2 of the two FSPs of the prototype model of the interferometer were set at 1.540 and 1.570 mm, respectively. As the input polarizer of the sideband separator, a fixed 45° wire-grid polarizer was installed at the input port to set the incident beam polarized at 45° with respect to the plane of incidence.

On the other hand, the output beam polarization was selected at either $+45°$ or $-45°$ to the plane of incidence by changing the orientation of a wire-grid polarizer to simulate the transmission

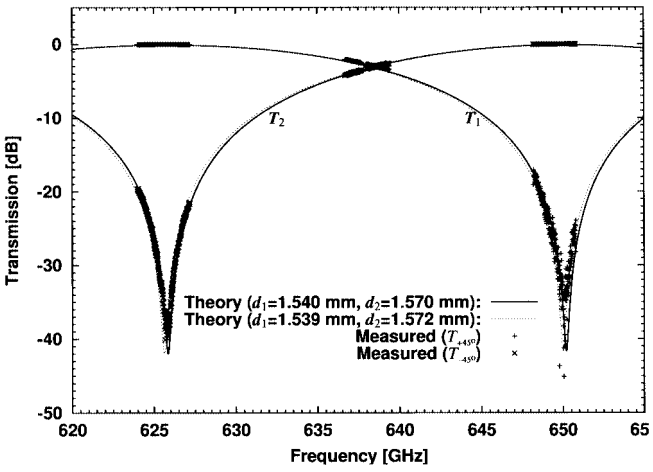

Fig. 6. Comparison of the measured and theoretically calculated transmission characteristics of the FSP-based sideband separator.

characteristics at orthogonally polarized output ports 1 and 2 of the sideband separator.

The transmission characteristics of this sideband separator were measured by using a submillimeter-wave vector network analyzer. The output of the phase-locked submillimeter-wave

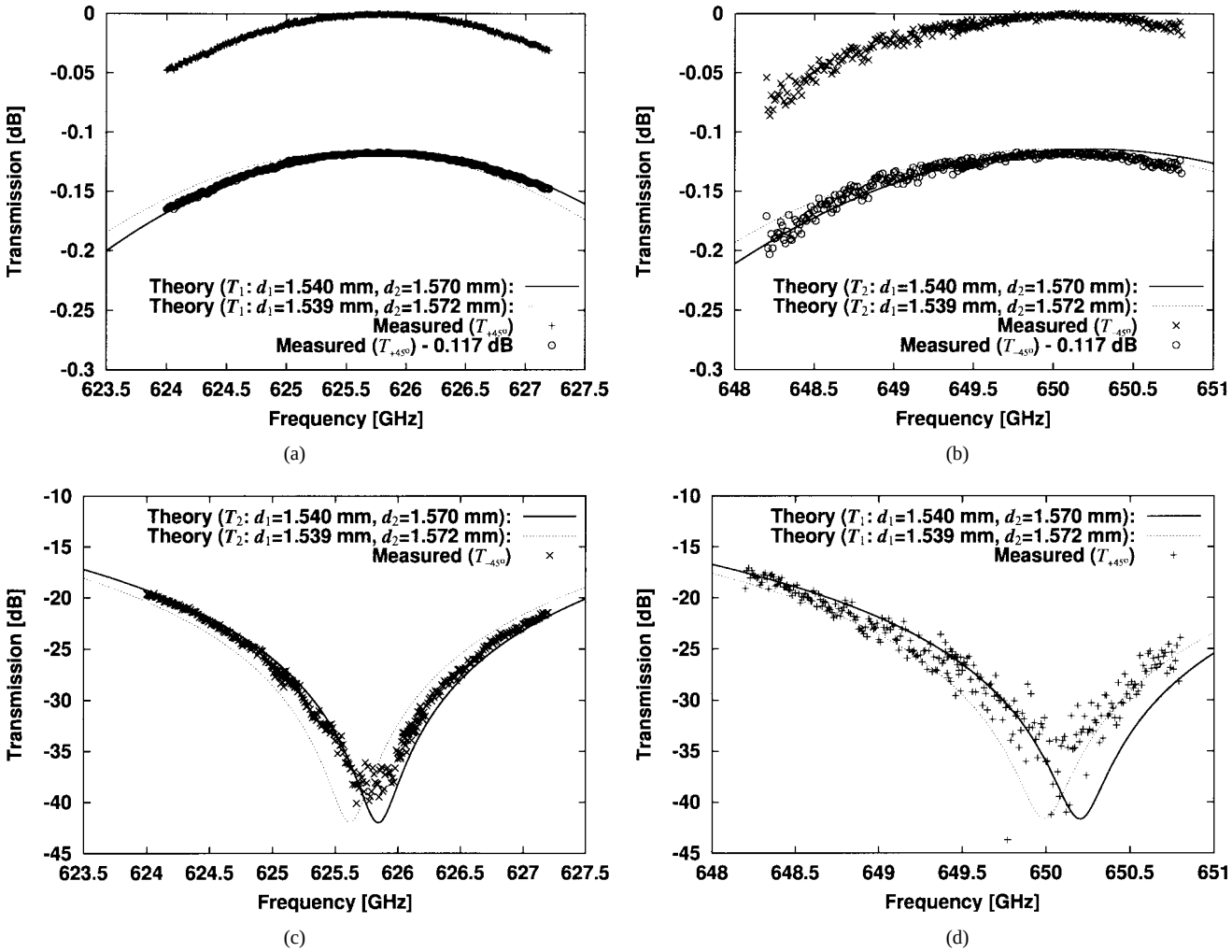

Fig. 7. Enlarged views of Fig. 6 for comparison of the measured and theoretically calculated characteristics of the FSP-based sideband separator. (a) Bandpass (b) and rejection characteristics around the LSB, and (c) bandpass and (d) rejection characteristics around the USB.

source was coupled to the device under test via a back-to-back corrugated feed horn.[2] The output of this feed horn was directed to an offset ellipsoidal reflector to form a collimated Gaussian beam with a beam-waist radius of 4.61 mm to be propagated through the sideband separator under test. At the output of the device under test, another offset ellipsoidal reflector was used to couple the output beam to the feed horn of the submillimeter-wave detector.

In this measurement configuration, standing waves due to the reflection between optical components such as the one between the source and back-to-back horn feeding the input beam is inevitable to some extent. Because of the ripples due to this residual standing waves, it was very hard to determine absolute values of very low transmission losses in the transmission bands of the sideband separator. Provided that the ripples in the measured transmission characteristics are caused by the standing waves generated outside of the interferometer, the standing-wave ripples should appear at both output polarizations with almost equal voltage standing-wave ratio (VSWR). To suppress the ripples due to these residual standing waves, the output amplitude V_{+45° and V_{-45° taken for output polarization at $+45^\circ$ and -45°, respectively, at the same frequency were normalized to estimate the transmission coefficient T_1 and T_2 for respective output polarizations with the following equations by neglecting small losses, most of which are ohmic losses in the FSP, common to both output polarizations:

$$T_{+45^\circ} = 10\log\frac{|V_{+45^\circ}|^2}{|V_{+45^\circ}|^2 + |V_{-45^\circ}|^2} \quad \text{(dB)} \qquad (10)$$

and

$$T_{-45^\circ} = 10\log\frac{|V_{-45^\circ}|^2}{|V_{+45^\circ}|^2 + |V_{-45^\circ}|^2} \quad \text{(dB)}. \qquad (11)$$

Besides this, the normalization is also needed to compensate the residual frequency dependence of the measurement system, which cannot be fully calibrated.

Since the measurements were made under an atmospheric pressure of approximately 950 hPa at room temperature, the measurement results should be compared with theoretical calculation taking the atmospheric refractivity into consideration.

[2]The use of a back-to-back horn here is not essential in the present measurement. This back-to-back horn and the ellipsoidal reflector had to be used for optical-design reason of quasi-optics of the JEM/SMILES system for which our interferometer was developed [8].

The atmospheric correction was made just by scaling the frequency of theoretical calculations by a factor of 1.0003^{-1} considering the atmospheric refractivity of 1.0003.

Transmission characteristics T_{+45° and T_{-45° measured for the fabricated FSP-based sideband separator around the LSB and USB of the JEM/SMILES receiver are compared with theoretically calculated T_1 and T_2 for the atmospheric condition in Figs. 6 and 7. In these comparisons, the measurement results are compared with the theoretical calculations for the designed FSP spacings ($d_1 = 1.540$ mm and $d_2 = 1.570$ mm), as well as those for the actually measured spacings ($d_1 = 1.539$ mm and $d_2 = 1.572$ mm) measured after fabrication of the FSPs. In Fig. 6, we can see an overall good agreement between the theory and measurement results. More detailed comparisons of characteristics around the transmission and rejection bands are shown in Fig. 7. Since the measured T_{+45° and T_{-45° are normalized by ignoring polarization independent loss, as has been mentioned before, it should be noted that we can directly compare only relative level variations of them with the theoretically calculated ones, in particular, in the transmission bands where the transmission loss is very low, as shown in Fig. 7(a) and (b). As is found in Fig. 7(a) and (b), if a slight offset of -0.117 dB is applied to the measured data, an excellent agreement is found between the measurements and theoretical calculations. The larger scatter of the data in the USB as compared with in the LSB is due to a degradation of the detector sensitivity.

These comparisons indicate that the transmission and rejection characteristics of the FSP-based interferometer can be designed and fabricated with a frequency accuracy better than $5 \cdot 10^{-4}$ based on theoretical calculations taking the effects of multiple reflection and diffraction into account.

VII. Conclusion

This paper has presented a new configuration of polarization-rotating dual-beam interferometer consisting of two FSPs each of which consists of a freestanding wire grid backed by a reflecting mirror. The detailed analysis of its characteristics is a little more complicated than the standard MPI due to the multiple reflection within the FSP. We have verified the analysis using a prototype model of a sideband separator based on the FSP-based interferometer operating in a submillimeter-wave band around 640 GHz. We have shown that its transmission characteristics can be designed by taking the effects of multiple reflection and diffraction into account, and that it can be fabricated with a frequency accuracy better than $5 \cdot 10^{-4}$ based on this design.

Appendix A
Reflection Characteristics of FSP for Plane Waves

Here, the amplitude reflection coefficient of the FSP is derived for plane-wave incidence by assuming that the wire grid of the FSP is a periodic array of conductive cylinders of radius a and pitch g and is backed by a flat mirror with a grid-mirror spacing of d.

Let us consider the case when a plane wave is incident with an angle of incidence θ on the FSP whose grid wires are oriented perpendicular to the plane of incidence, as shown in Fig. 8.

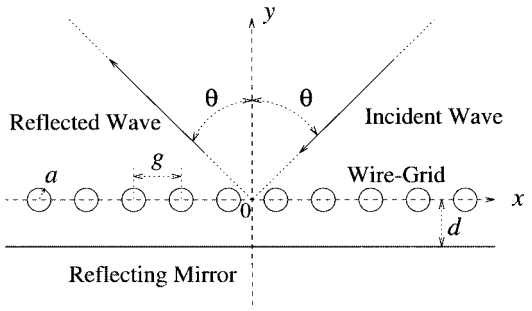

Fig. 8. Configuration of the FSP.

By taking the multiple reflection between the wire grid and mirror into account, the complex amplitude reflection coefficient of the FSP for s- or p-polarization is given by[3]

$$R = r + \frac{r_m t^2 \exp(i\phi)}{1 - r_m r \exp(i\phi)} \tag{12}$$

with

$$\phi = \frac{4\pi d \cos\theta}{\lambda} \tag{13}$$

where λ is the wavelength and d is the spacing between the grid and the mirror. In (12), r and t are the complex amplitude reflection and transmission coefficients of the wire grid, and r_m is the complex reflection coefficient of the reflecting mirror. If the mirror is made of metal with a finite conductivity of σ_m, r_m is given by

$$r_m = \frac{\cos\theta - \sqrt{i\frac{\sigma_m}{2\pi f \varepsilon_0} - \sin^2\theta}}{\cos\theta + \sqrt{i\frac{\sigma_m}{2\pi f \varepsilon_0} - \sin^2\theta}} \tag{14}$$

for s-polarization and

$$r_m = -\frac{\sqrt{i\frac{\sigma_m}{2\pi f \varepsilon_0} - \sin^2\theta} - i\frac{\sigma_m}{2\pi f \varepsilon_0}\cos\theta}{\sqrt{i\frac{\sigma_m}{2\pi f \varepsilon_0} - \sin^2\theta} + i\frac{\sigma_m}{2\pi f \varepsilon_0}\cos\theta} \tag{15}$$

for p-polarization. On the other hand, the complex amplitude reflection coefficient r and transmission coefficient t for a wire grid consisting of cylinders with finite conductivity can be obtained by the efficient calculation method given in Appendix B.

Appendix B
Transmission and Reflection Coefficients of Wire Grid With Finite Conductivity

Transmission and reflection characteristics of plane waves impinging on a wire grid consisting of parallel conducting cylinders with circular cross section can be calculated by the efficient method proposed by Kushta and Yasumoto [12] and Yasumoto and Yoshitomi [13].

[3]See footnote 1 in Section V of this paper.

For a wire grid with $g(1+\sin\theta) < \lambda$, the complex amplitude reflection coefficient r and the complex amplitude transmission coefficient t of the wire grid are given by

$$r = \boldsymbol{p}_0^T \cdot \boldsymbol{a}_0^{sc} \tag{16}$$

and

$$t = 1 + \boldsymbol{q}_0^T \cdot \boldsymbol{a}_0^{sc} \tag{17}$$

respectively, with

$$\boldsymbol{p}_0 = \begin{bmatrix} \dfrac{2(-i)^m (k_x + ik_y)^m}{k_y k_0^m g} & (m \geq 0) \\ \dfrac{2i^{|m|}(k_x - ik_y)^{|m|}}{k_y k_0^{|m|} g} & (m < 0) \end{bmatrix} \tag{18}$$

and

$$\boldsymbol{q}_0 = \begin{bmatrix} \dfrac{2(-i)^m (k_x - ik_y)^m}{k_y k_0^m g} & (m \geq 0) \\ \dfrac{2i^{|m|}(k_x + ik_y)^{|m|}}{k_y k_0^{|m|} g} & (m < 0) \end{bmatrix} \tag{19}$$

where $k_0 = 2\pi/\lambda$, $k_x = -k_0 \sin\theta$, $k_y = \sqrt{k_0^2 - k_x^2}$, $\boldsymbol{a}^{sc}$ is the column vector of the scattering amplitude, and the superscript T denote the transpose of the indicated vector.

The scattering amplitude $\boldsymbol{a}^{sc}$ in (16) and (17) is given by

$$\boldsymbol{a}_0^{sc} = (\boldsymbol{I} - \boldsymbol{T} \cdot \boldsymbol{L})^{-1} \cdot \boldsymbol{T} \cdot \boldsymbol{a}^{in} \tag{20}$$

where T is the T-matrix for isolated grid wire, $\boldsymbol{L}$ is the square matrix whose elements are related with the lattice sums for periodic Green's function [14], $\boldsymbol{I}$ is the identity matrix, and $\boldsymbol{a}^{in}$ is the column vector whose mth component is given by $(-1)^m e^{im\theta}$. The elements of $\boldsymbol{L}$ are given by semi-infinite lattice sums of the Hankel function of the first kind ($H_n^{(1)}$) as follows [14]:

$$L_{mn} = S_{m-n}(k_0 g, \theta) \tag{21}$$

$$S_n(k_0 g, \theta) = \sum_{l=1}^{\infty} H_n^{(1)}(lk_0 g) e^{-ilk_0 g \sin\theta} + (-1)^n \sum_{l=1}^{\infty} H_n^{(1)}(lk_0 g) e^{ilk_0 g \sin\theta}. \tag{22}$$

It is well known that the convergence of the direct sum in (22) is desperately slow. To overcome this slow convergence, Yasumoto and Yoshitomi invented an integral form of the lattice sums for efficient calculation [13] given as follows:

$$\sum_{l=1}^{\infty} H_n^{(1)}(lk_0 g) e^{\mp ilk_0 g \sin\theta} = \frac{(-1)^n}{\pi} e^{-i(\pi/4 \pm k_0 g \sin\theta)} \times \int_0^u \left[G_n(\tau) + G_n(-\tau)\right] \times F(\tau; k_0 g \mp \sin\theta) dt \tag{23}$$

with

$$G_n(\tau) = (\tau + i\sqrt{1-\tau^2})^n \tag{24}$$

$$F(\tau; k_0 g \mp \sin\theta) = \frac{e^{ik_0 g\sqrt{1-\tau^2}}}{\sqrt{1-\tau^2}\left[1 - e^{ik_0 g(\sqrt{1-\tau^2} \mp \sin\theta)}\right]} \tag{25}$$

where $\tau = (1-i)/\sqrt{2}$ and u is a positive real number chosen so that the integration satisfies a required convergence.

The T-matrix for the conducting grid wire with circular cross section made of metal with finite conductivity is given by a diagonal matrix whose matrix elements T_{mn} are given by

$$T_{mn} = -\delta_{mn} \frac{k_g J_m(k_0 a) J_m'(k_g a) - k_0 J_m(k_g a) J_m'(k_0 a)}{k_g J_m'(k_g a) H_m^{(1)}(k_0 a) - k_0 J_m(k_g a) H_m'^{(1)}(k_0 a)} \tag{26}$$

for s-polarization and

$$T_{mn} = -\delta_{mn} \frac{k_0 J_m(k_0 a) J_m'(k_g a) - k_g J_m(k_g a) J_m'(k_0 a)}{k_0 J_m'(k_g a) H_m^{(1)}(k_0 a) - k_g J_m(k_g a) H_m'^{(1)}(k_0 a)} \tag{27}$$

for p-polarization with

$$k_g = k_0 \sqrt{i \frac{\sigma_g}{2\pi f \varepsilon_0}} \tag{28}$$

where a is the radius of the grid wire and σ_g is the conductivity of the cylinder.

ACKNOWLEDGMENT

The authors would like to thank Prof. K. Yasumoto, Kyushu University, Fukuoka-shi, Japan, for his elucidating comments and discussions on electromagnetic scattering calculations for wire grids with the use of an efficient calculation method that utilizes the lattice sums and T-matrix developed by him.

REFERENCES

[1] P. F. Goldsmith, "Quasi-optical technologies at millimeter and submillimeter wavelengths," in *Infrared and Millimeter Waves*, K. J. Button, Ed. New York: Academic, 1982, vol. 6, pp. 277–343.

[2] J. W. Archer, "Low-noise heterodyne receivers for near-millimeter-wave radio astronomy," *Proc. IEEE*, vol. 73, pp. 109–130, Jan. 1985.

[3] N. R. Erickson, "A very low-noise single-sideband receiver for 200–260 GHz," *IEEE Trans. Microwave Theory Tech.*, vol. MTT-33, pp. 1179–1188, Nov. 1985.

[4] ——, "A new quasi-optical filter: The reflective polarizing interferometer," *Int. J. Infrared Millim. Waves*, vol. 8, pp. 1015–1025, 1987.

[5] C. E. Tong and R. Blundell, "A quasi-optical image separation scheme for millimetre and submillimetre waves," *IEEE Trans. Microwave Theory Tech.*, vol. 42, pp. 2174–2177, Nov. 1994.

[6] D. H. Martin and E. Puplett, "Polarized interferometric spectrometry for the millimeter and submillimeter spectrum," *Infrared Phys.*, vol. 10, pp. 105–109, 1969.

[7] D. H. Martin, "Polarizing (Martin–Puplett) interferometric spectrometers for the near- and submillimeter spectra," in *Infrared and Millimeter Waves*, K. J. Button, Ed. New York: Academic, 1982, vol. 6, pp. 65–148.

[8] J. Inatani, H. Ozeki, R. Satoh, T. Nishibori, N. Ikeda, Y. Fujii, T. Nakajima, Y. Iida, T. Iida, K. Kikuchi, T. Miura, H. Masuko, T. Manabe, S. Ochiai, M. Seta, Y. Irimajiri, Y. Kasai, M. Suzuki, T. Shirai, S. Tsujimaru, K. Shibasaki, and M. Shiotani, "Submillimeter limb-emission sounder JEM/SMILES aboard the space station," presented at the 2nd Int. SPIE Asia–Pacific Symp. on Remote Sensing of Atmosphere, Environment, and Space, Sendai, Japan, Oct. 9–12, 2000.

[9] (2002) JEM/SMILES Mission Plan. SMILES Sci. Team, Committee for Earth Observation Syst., Earth Sci. Technol. Forum, Tokyo, Japan. [Online]. Available: http://www.crl.go.jp/dk/c214/smiles/Mission_Plan/

[10] *Chronological Scientific Tables (Rika Nenpyo)* (in Japanese), Nat. Astronomical Observatory, Tokyo, Japan, 2000, p. 482.

[11] P. F. Goldsmith, *Quasioptical System*. Piscataway, NJ: IEEE Press, 1998, pp. 63–67.
[12] K. Kushta and K. Yasumoto, "Electromagnetic scattering from periodic arrays of two circular cylinders per unit cell," *Progress Electromagn. Res. PIERS*, vol. 29, pp. 69–85, 2000.
[13] K. Yasumoto and K. Yoshitomi, "Efficient calculation of lattice sums for free-space periodic Green's function," *IEEE Trans. Antennas Propagat.*, vol. 47, pp. 1050–1055, June 1999.
[14] N. A. Nicorovici and R. C. McPhedran, "Lattice sums for off-axis electromagnetic scattering by gratings," *Phys. Rev. E, Stat. Phys. Plasmas Fluids Relat. Interdiscip. Top.*, vol. 50, no. 4, pp. 3143–3160, Oct. 1994.

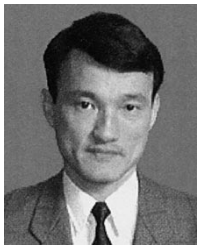

Takeshi Manabe (M'88) was born in Osaka, Japan, on September 19, 1952. He received the B.S., M.S., and D.E. degrees in electronics engineering from Kyoto University, Kyoto, Japan, in 1975, 1977, and 1980, respectively.

In 1980, he joined the Radio Research Laboratory, Ministry of Posts and Telecommunications, Tokyo, Japan, where he has been engaged in research on radio-wave propagation characteristics of centimeter and millimeter waves in the atmosphere. From 1986 to 1987, he was a Visiting Scientist with the National Telecommunications and Information Administration, Institute for Telecommunication Sciences, Boulder, CO. From 1988 to 1991, he was with the ATR Optical and Radio Communications Research Laboratories, Kyoto, Japan, where he was engaged in research on antenna array signal processing and indoor radio propagation. Since 1991, he has been with the Communications Research Laboratory, Tokyo, Japan. His current research interests include microwave and millimeter-wave propagation and remote sensing. He is currently involved in research and development of the submillimeter-wave limb-emission sounder (SMILES) to be aboard the Japanese Experiment Module (JEM) of the International Space Station for observing stratospheric minor constituents related to ozone depletion.

Dr. Manabe is a member of the Institute of Electronics, Information and Communication Engineers (IEICE), Japan, and the Physical Society of Japan. He is a secretary of the Japanese National Committee of the International Union of Radio Science (URSI), Commission F.

Junji Inatani received the B.S. degree in physics from Kyoto University, Kyoto, Japan, in 1972, and the M.S. and Ph.D. degrees in astronomy from the University of Tokyo, Tokyo, Japan, in 1974 and 1979, respectively.

In 1980, he joined the Nobeyama Radio Observatory, Nagano, Japan, which was founded as a radio astronomy facility at the Tokyo Astronomical Observatory (TAO), University of Tokyo. He had been engaged in research and developments of millimeter-wave receivers based on superconductive devices, for the 45-m Telescope and Nobeyama Millimeter Array. The TAO was reorganized to the National Astronomical Observatory (NRO) of Japan in 1988. From 1992 to 1997, he was the Director of the NRO, where he was responsible for the promotion of radio astronomy research and open-use operations of the facility. He also contributed to developments of the submillimeter-wave telescope atop Mount Fuji. In 1997, he joined the National Space Development Agency of Japan, Ibaraki, Japan, where he has been the leader of the development of submillimeter-wave limb-emission sounder (SMILES), which is to be aboard the Japanese Experiment Module (JEM) of the International Space Station for observing stratospheric minor constituents related to ozone depletion.

Axel Murk was born in Germany, in 1968. He received the M.S. degree in physics from the Technical University of Munich, Munich, Germany, in 1995, and the Ph.D. degree in physics from the University of Bern, Bern, Switzerland, in 1999.

Since then, he has been involved in the characterization of submillimeter-wave instrumentation for different space projects, including the qualification tests of the input optics for the submillimeter-wave limb-emission sounder (SMILES).

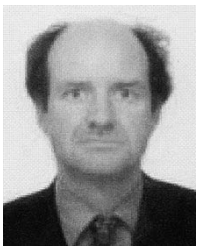

Richard J. Wylde was born in London, U.K., on February 15, 1958. He received the B.A. degree in natural sciences from Sidney Sussex College, Cambridge, U.K., in 1979, and the Ph.D. degree in physics from Queen Mary and Westfield (now Queen Mary) College, University of London, London, U.K., in 1985.

Since then, he has split his time between academic work, currently as an Honorary Reader with the School of Physics and Astronomy, University of St. Andrews, Fife, U.K., and managing both Thomas Keating Ltd., Precision Engineers, and QMC Instruments Ltd., manufacturers of cooled terahertz detectors. His research interests lie in the design of terahertz optics for use in plasma diagnostics, cosmology, astronomy, electron spin resonance spectroscopy, and atmospheric remote sensing.

Masumichi Seta received the B.A. degree in natural science from the International Christian University, Tokyo, Japan, in 1991, the M.Eng. degree in electromagnetic energy engineering from Osaka University, Osaka, Japan, in 1993, and the Dr.Sci. degree in astronomy from The University of Tokyo, Tokyo, Japan, in 1996.

From 1996 to 1997, he was with the I. Phyisikalishes Institut, Universität zu Köln, Cologne, Germany, as a Post-Doctoral Fellow of the Japan Society of the Promotion of Science. In 1997, he joined the Communications Research Laboratory, Tokyo, Japan, where he has been engaged in research and development of the submillimeter-wave receiver system for submillimeter-wave limb-emission sounder (SMILES) to be aboard the Japanese Experiment Module (JEM) of the International Space Station for observing stratospheric minor constituents related to ozone depletion.

Derek H. Martin received the B.S. degree in physics and Ph.D. from the University of Nottingham, Nottingham, U.K., in 1950 and 1954, respectively.

Since then, he has been with Queen Mary, University of London, London, U.K., where he became a Professor of physics in 1970, Emeritus Professor in 1994, and Honorary Fellow in 1995. He was Editor of *Advances in Physics* (1973–1983). His research interests were initially in experimental studies of ferromagnetism and superconductivity and subsequently in the development of techniques for detecting and analyzing terahertz electromagnetic waves, and in using those techniques in spectroscopic studies of collective excitations in solids, the molecular constituents of the stratosphere, the cosmic microwave background spectrum, and plasma diagnostics.

Dr. Martin is a Fellow of the Institute of Physics, of which he was honorary secretary (1984–1994). He was the recipient of the 1983 Metrology Award of the U.K. National Physical Laboratory and the 1992 SPIE Kenneth J. Button Prize for his contributions to terahertz measurement techniques including polarization interferometry.